Interaction between a gold substrate and monolayer MoS_2: An azimuthal-dependent sum frequency generation study

Tao Yang [1,*] Erik Pollmann [1] Stephan Sleziona [1] Eckart Hasselbrink [2] Peter Kratzer [1] Marika Schleberger [1] R. Kramer Campen [1] and Yujin Tong [1,†]

[1] *Faculty of Physics, University of Duisburg-Essen, 47057 Duisburg, Germany*

[2] *Faculty of Chemistry, University of Duisburg-Essen, 45117 Essen, Germany*

(Received 24 November 2022; revised 4 April 2023; accepted 7 April 2023; published 27 April 2023)

Most of the monolayer transition metal dichalcogenides (TMDCs) are chemically stable and have a combination of electronic, linear, and nonlinear optical (NLO) characteristics not generally found in bulk solids. This combination of traits has driven intense interest in their application in a variety of optoelectronic and (photo)electrocatalytic contexts. To realize these applications, it is often necessary to bring the TMDC monolayer into contact with a metal surface. However, while the interaction between TMDCs and dielectric substrates has been intensely studied, much less has been reported on the interaction between TMDCs and metals. Here we use azimuthal-dependent sum frequency generation (SFG) spectroscopy to study the interaction of monolayer MoS_2 and gold by comparing the second-order NLO response of MoS_2 on Si/SiO_2 as a function of azimuthal angle. In contrast to the well-known sixfold symmetric pattern of MoS_2 on Si/SiO_2 in all polarization combinations, both the symmetric pattern and relative intensities of the azimuthal-dependent SFG response of MoS_2 on Au depend strongly on polarization. Analysis of the components and magnitudes of the second-order nonlinear susceptibility ($\chi^{(2)}$) of the MoS_2/SiO_2, MoS_2/Au, and gold substrate reveals a strong interaction between monolayer MoS_2 and gold substrate broadly consistent with prior theoretical studies. Our measurement of the photon energy dependent nonlinear optical signal symmetry on MoS_2/Au is strong evidence that we observe a mode-specific electronic effect that depends on the exciton resonance. In addition our approach allows the quantification of the $\chi^{(2)}$ of monolayer MoS_2 on SiO_2 and Au, $(7.9 \pm 1.6) \times 10^{-20}$, and $(1.4 \pm 0.3) \times 10^{-19}$ m^2/V, respectively. The current study demonstrates that the interaction between Au and a model TMDC monolayer substantially alters both the magnitude and symmetry of the NLO response. Such effects are important in application of these materials in optoelectronic devices and offer a contact-free probe of substrate-induced changes in the monolayer's electronic structure.

DOI: 10.1103/PhysRevB.107.155433

I. INTRODUCTION

Transition metal dichalcogenides (TMDCs) are promising candidates for optoelectronics [1,2], nonlinear optics [3,4], and photocatalysis [5,6] because of their direct band gap in the visible to near-infrared, large and ultrafast nonlinear optical (NLO) response, pronounced activity for photoelectrochemical water splitting, and reasonable stability in ambient conditions. Taking advantage of these properties to fabricate TMDC-based devices and catalysts, however, usually requires TMDC/metal heterostructures in which, for example, the metal surface acts as an electron collector. Since most monolayer TMDCs are semiconductors, a semiconductor-metal junction will form when a TMDC is in contact with a metal material. In this hybrid system, the metal-semiconductor interaction plays an important role in the performance of the aforementioned devices. The influences are reflected in the charge transfer rate across the interface [7,8], contact resistance [9–11], and strength of optical response [12,13]. Although many efforts have been made to reduce contact resistance [14–17] and design various metal nanostructures to achieve high quantum efficiency [18], little is known about how the metal substrates affect the optical, especially the NLO, response of TMDCs. In this study we address these questions for the model system molybdenum disulfide (MoS_2) on gold.

The optical response of a TMDC in general, e.g., MoS_2, is determined by its electronic and geometric structure. When monolayer MoS_2 is optically excited with photons of energy near the band gap, a bound electron-hole pair, i.e., an exciton, is directly created. Because the electric field between the electron and hole is poorly screened in the monolayer, binding energies of these excitons are quite high relative to bulk values. In addition, strong spin-orbit coupling results in the splitting of the valence band edge. These two properties result in two peaks in the absorption [19] and photoluminescence [20,21] spectra: the *A* and *B* exciton. For freestanding monolayer MoS_2, the peaks of the *A* and *B* exciton spectral response have been reported to be ≈1.8–1.9 and ≈2.0–2.1 eV, respectively [20,22]. Putting MoS_2 on a metal virtually completely quenches both features in photoluminescence spectra [7,23,24]. In contrast, both features in a linear optical

*tao.yang@uni-due.de
†yujin.tong@uni-due.de

absorption spectrum are less affected by the monolayer-metal interaction [25,26]. To the best of our knowledge, there is no report on how the NLO response may be affected by the sample-substrate interaction.

The design of optoelectronic devices based on the nonlinear response of TMDCs requires direct knowledge of the symmetry of the NLO response (as described in detail below the symmetry determines the number of independent, and nonzero, terms in the nonlinear susceptibility). Additionally, the symmetry of the optical response is intimately related to the symmetry of the electronic and geometric structure: measuring the symmetry of the NLO response offers direct local structural insight [27–31]. On the one hand, the Coulomb interaction between an excited electron and hole has spherical symmetry. On the other, the lattice of freestanding monolayer TMDC has D_{3h} symmetry. It is unclear how these two symmetries might be expected to relate to the symmetry of the optical response. Unfortunately, the in-plane azimuthal symmetry cannot be probed via linear spectroscopy.

In previous second harmonic generation (SHG) studies—in which MoS_2 is irradiated with photons of energy ω and the emission with energy 2ω measured—a sixfold symmetric pattern has been reported for monolayer MoS_2 on a dielectric substrate [32–35]. There are no reported SHG studies of this system on a metal substrate. Here we employ a generalized version of SHG, the so-called sum frequency generation (SFG), to probe monolayer MoS_2 on two types of substrates in the *A* and *B* exciton region. Because SFG is a coherent second-order NLO response, it overcomes many of the challenges described above. To better understand the interesting substrate-dependent SFG results, in Sec. II, we will first present the basic theory of SFG and the relationship between macroscopic susceptibility and hyperpolarizability components in azimuthal-dependent SFG measurements. Then we will discuss the NLO responses of two sample systems belonging to different point groups, D_{3h} and C_{3v}, based on their symmetry-allowed components.

II. THEORETICAL BACKGROUND

When light of frequency ω and wave vector $\vec{E}$ irradiates matter, the molecular scale response can be written as

$$\vec{\mu} = \alpha \cdot \vec{E}_\omega + \beta : \vec{E}_\omega \vec{E}_\omega + \gamma \vdots \vec{E}_\omega \vec{E}_\omega \vec{E}_\omega + \cdots, \tag{1}$$

in which $\vec{\mu}$ is the induced dipole, α is the polarizability, and β and γ are the first- and second-order hyperpolarizabilities. The first term on the right hand side of Eq. (1) is the source term for linear optical processes: linear light scattering, infrared absorption, etc. The second term is the source of second-order nonlinear optical processes: sum and difference frequency generation, second harmonic generation, and optical rectification. The third term and the rest of it are the sources of high-order nonlinear optical processes.

The linear polarizability, α, can be expressed as a 3×3 matrix. For the case of MoS_2, which has local D_{3h} symmetry, α is (where z is parallel to the crystallographic c axis)

$$\begin{bmatrix} \alpha_{xx} & 0 & 0 \\ 0 & \alpha_{yy} & 0 \\ 0 & 0 & \alpha_{zz} \end{bmatrix}, \tag{2}$$

in which $\alpha_{xx} = \alpha_{yy}$. This last equality implies that there can be no in-plane azimuthal-dependent linear optical response: the in-plane macroscopic susceptibility (defined below) does not depend on orientation.

The hyperpolarizability, β, is the source of the second nonlinear material response and can be expressed as a 3×9 matrix. For a material with D_{3h} symmetry, β can be written as

$$\begin{bmatrix} 0 & \beta_{xyx} & 0 & \beta_{xxy} & 0 & 0 & 0 & 0 & 0 \\ \beta_{yxx} & 0 & 0 & 0 & \beta_{yyy} & 0 & 0 & 0 & 0 \\ 0 & 0 & 0 & 0 & 0 & 0 & 0 & 0 & 0 \end{bmatrix}, \tag{3}$$

in which there is only one independent term, i.e., $\beta_{yyy} = -\beta_{xyx} = -\beta_{xxy} = -\beta_{yxx}$. When symmetry is lifted, e.g., $D_{3h} \rightarrow C_{3v}$, the hyperpolarizability tensor now becomes

$$\begin{bmatrix} 0 & \beta_{xyx} & \beta_{xzx} & \beta_{xxy} & 0 & 0 & \beta_{xxz} & 0 & 0 \\ \beta_{yxx} & 0 & 0 & 0 & \beta_{yyy} & \beta_{yzy} & 0 & \beta_{yyz} & 0 \\ \beta_{zxx} & 0 & 0 & 0 & \beta_{zyy} & 0 & 0 & 0 & \beta_{zzz} \end{bmatrix}, \tag{4}$$

in which, as for D_{3h}, $\beta_{yyy} = -\beta_{xyx} = -\beta_{xxy} = -\beta_{yxx}$ but now also $\beta_{xzx} = \beta_{yzy}$, $\beta_{xxz} = \beta_{yyz}$, $\beta_{zxx} = \beta_{zyy}$ and β_{zzz}. That is, there are now five nonzero and independent terms.

Measurements of SFG (or SHG) characterize the *macroscopic* induced polarization ($\vec{P}$). The macroscopic analog of Eq. (1) is

$$\vec{P} = \epsilon_0[\chi^{(1)} \cdot \vec{E}_\omega + \chi^{(2)} : \vec{E}_\omega \vec{E}_\omega + \chi^{(3)} \vdots \vec{E}_\omega \vec{E}_\omega \vec{E}_\omega + \cdots], \tag{5}$$

where $\chi^{(i)}$ is the ith order (non)linear optical susceptibility. As has been described by prior authors, and we review in the Supplemental Material [36], the polarizability, hyperpolarizability, and second-order hyperpolarizability can be related to the analogous $\chi^{(i)}$'s by a Euler transformation. The nonlinear optical susceptibility tensors of D_{3h} and C_{3v} point groups can be found in the Supplemental Material [36]. Given a D_{3h} sample oriented with respect to the laboratory reference frame as shown in Fig. 1 and independent control over the polarization of each beam (p = parallel to the plane of incidence and s = perpendicular), each of the eight possible polarization combinations can be related to the macroscopic susceptibility and hyperpolarizability components as shown in Table I. Sum frequency (or second harmonic) intensities are proportional to the squared modulus of the macroscopic second-order susceptibility. The relationships shown in Table I clearly show that, for all possible polarization conditions of a sample with microscopic D_{3h} symmetry oriented in the laboratory frame as shown in Fig. 1, one would expect to observe

$$I_{\mathrm{SFG}} \propto \left| \pm \chi^{(2)}_{YYY} \sin(3\theta) \right|^2 \quad \text{or} \quad I_{\mathrm{SFG}} \propto \left| \pm \chi^{(2)}_{YYY} \cos(3\theta) \right|^2, \tag{6}$$

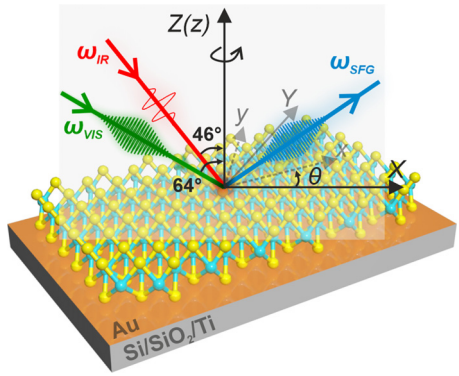

FIG. 1. Schematic diagram of our experiment. Exfoliated monolayer MoS_2 on Au was investigated by the azimuthal-dependent SFG. Laboratory coordinates (*X, Y, Z*) and molecular coordinates (*x, y, z*) were used to describe the system. *X (x)* and *Y (y)* axes are parallel to the sample plane, while the *Z (z)* axis is perpendicular to the *X-Y (x-y)* plane. The three beams, visible (ω_{VIS}), infrared (ω_{IR}), and SFG (ω_{SFG}), are coplanar in the *X-Z* plane. The *x (y)* axis is parallel (perpendicular) to the zigzag direction of the MoS_2 monolayer. The θ is the azimuthal angle and its physical meaning is the rotational angle of zigzag direction (i.e., the *x* axis in the molecular frame) of the MoS_2 monolayer with respect to the incident plane of the lasers (i.e., the *X* axis) in the laboratory frame.

where I_{SFG} is the SFG intensity and θ is the azimuthal angle. Below we demonstrate that I_{SFG} for MoS_2 on a dielectric substrate has the expected sixfold symmetric pattern with a polarization-dependent 30° offset. Note that while these simplified signal expressions are sufficient to describe the azimuthal symmetry of the measured I_{SFG}, to describe intensity ratios requires accounting for the Fresnel coefficients (see the Supplemental Material for the full expression [36]).

When monolayer MoS_2 is placed on the metal substrate, e.g., gold, the D_{3h} symmetry can be lifted to C_{3v} because the strong interaction between them results in symmetry breaking (details will be discussed in Sec. III). For samples with microscopic C_{3v} symmetry [31], Eq. (4) clearly shows we might expect a more complicated macroscopic response.

TABLE I. Relationship of measurement condition (where *pss* indicates *p* polarized SFG, *s* polarized visible, and *s* polarized infrared light beams), second-order macroscopic susceptibility ($\chi^{(2)}_{IJK}$), and hyperpolarizability (β_{ijk}) components for a sample belonging to the D_{3h} point group.

Polarization combination	Nonzero $\chi^{(2)}_{IJK}$	Nonzero β_{ijk}
spp	$\chi^{(2)}_{YXX}$	$-\beta_{yyy}\cos(3\theta)$
ssp	$\chi^{(2)}_{YYX}$	$-\beta_{yyy}\sin(3\theta)$
sps	$\chi^{(2)}_{YXY}$	$-\beta_{yyy}\sin(3\theta)$
sss	$\chi^{(2)}_{YYY}$	$\beta_{yyy}\cos(3\theta)$
ppp	$\chi^{(2)}_{XXX}$	$\beta_{yyy}\sin(3\theta)$
psp	$\chi^{(2)}_{XYX}$	$-\beta_{yyy}\cos(3\theta)$
pps	$\chi^{(2)}_{XXY}$	$-\beta_{yyy}\cos(3\theta)$
pss	$\chi^{(2)}_{XYY}$	$-\beta_{yyy}\sin(3\theta)$

TABLE II. Relationship of measurement condition, second-order macroscopic susceptibility ($\chi^{(2)}_{IJK}$), and hyperpolarizability (β_{ijk}) components for a sample belonging to the C_{3v} point group.

Polarization combination	Nonzero $\chi^{(2)}_{IJK}$	Nonzero β_{ijk}
spp	$\chi^{(2)}_{YXX}$	$-\beta_{yyy}\cos(3\theta)$
ssp	$\chi^{(2)}_{YYX}$	$-\beta_{yyy}\sin(3\theta)$
	$\chi^{(2)}_{YYZ}$	β_{xxz}
sps	$\chi^{(2)}_{YXY}$	$-\beta_{yyy}\sin(3\theta)$
	$\chi^{(2)}_{YZY}$	β_{xzx}
sss	$\chi^{(2)}_{YYY}$	$\beta_{yyy}\cos(3\theta)$
ppp	$\chi^{(2)}_{XXX}$	$\beta_{yyy}\sin(3\theta)$
	$\chi^{(2)}_{XXZ}$	β_{xxz}
	$\chi^{(2)}_{XZX}$	β_{xzx}
	$\chi^{(2)}_{ZXX}$	β_{zxx}
	$\chi^{(2)}_{ZZZ}$	β_{zzz}
psp	$\chi^{(2)}_{XYX}$	$-\beta_{yyy}\cos(3\theta)$
pps	$\chi^{(2)}_{XXY}$	$-\beta_{yyy}\cos(3\theta)$
pss	$\chi^{(2)}_{XYY}$	$-\beta_{yyy}\sin(3\theta)$
	$\chi^{(2)}_{ZYY}$	β_{zxx}

Appropriate transformation gives the values tabulated in Table II. In addition to the azimuthal-dependent terms for the D_{3h} symmetric sample shown in Table I, there are four additional unique nonzero terms, i.e., $\beta_{xzx} = \beta_{yzy}$, $\beta_{xxz} = \beta_{yyz}$, $\beta_{zxx} = \beta_{zyy}$, and β_{zzz}, that appear in four of the eight possible polarization combinations, i.e., *ppp*, *ssp*, *sps*, and *pss*. The measured signals are thus of the form

$$I_{\mathrm{SFG}} \propto |A \pm B\cos(3\theta)|^2 \quad \text{or} \quad I_{\mathrm{SFG}} \propto |A \pm B\sin(3\theta)|^2. \tag{7}$$

Such a signal generally exhibits a threefold pattern although the details depend, as shown below, on the relative sizes of the *A* and *B* terms. While both SHG and SFG sample the same material property, i.e., the frequency-dependent $\chi^{(2)}$, the information contained in the SFG response is potentially higher. In a typical degenerate SHG experiment, matter, in this case MoS_2, is irradiated with laser light of frequency ω, i.e., a single beam, and the intensity of the field emitted at 2ω is detected. Thus for the single-beam SHG experiment, there are only four unique polarization combinations: *ppp*, *pss*, *spp*, and *sss*. As noted above, for material with microscopic C_{3v} symmetry, there are *five* independent hyperpolarizability components. As a consequence, single-beam SHG is not sufficient to fully constrain the C_{3v} point group symmetry. For the SFG experiment two incident beams are typically employed with frequencies ω_1 and ω_2 and the intensity of the field at the *sum* of the frequencies, i.e., $\omega_1 + \omega_2 = \omega_{1+2}$, is detected. SFG, as tabulated above, therefore allows sampling eight polarization combinations and thus overcomes this limitation. Because the goal of our study is to probe the substrate-dependent change in $\chi^{(2)}$ from MoS_2, we therefore here employ SFG.

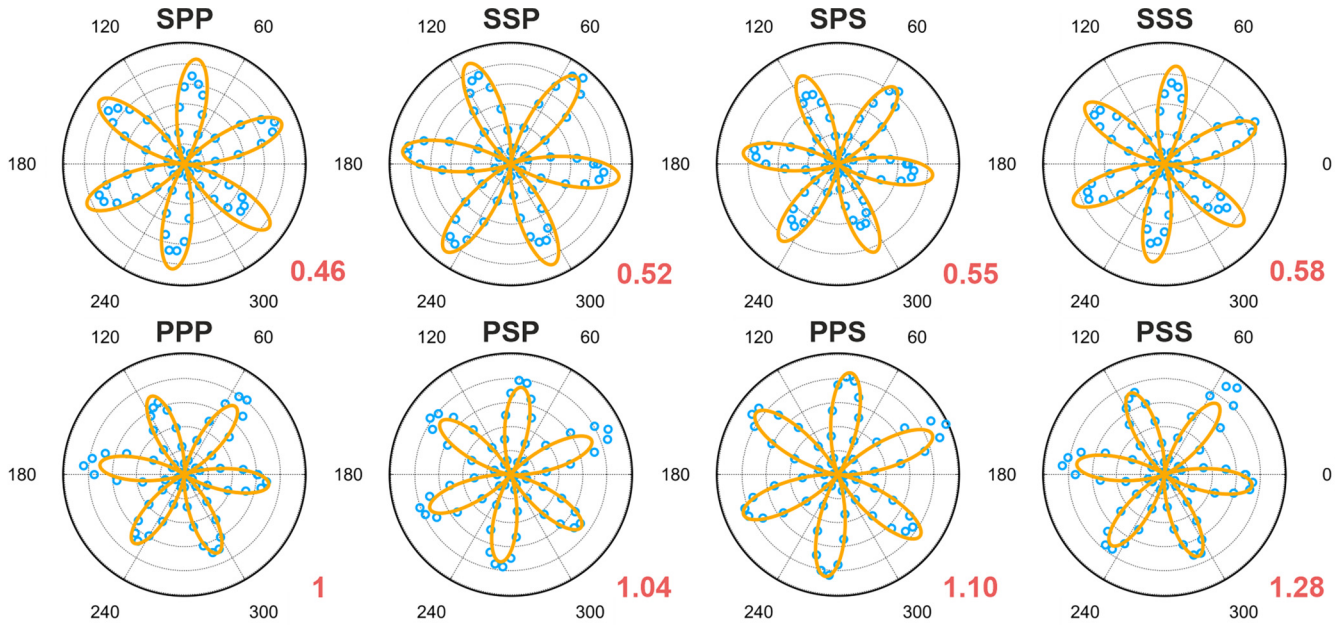

FIG. 2. Azimuthal-dependent SFG intensity of CVD-grown monolayer MoS_2 on a SiO_2 substrate under different polarization combinations. The blue circles represent the integrated intensity at specific rotation angles and the yellow solid lines are the global fitting results. The numbers in the lower right are the relative ratios of the maximum intensity to that of the *ppp* polarization.

III. RESULTS AND DISCUSSION

In this study, azimuthal-dependent signals I_{SFG} from monolayer MoS_2 on SiO_2/Si and on physical vapor deposited (PVD) gold (with a thickness of 25 nm) were collected. Monolayer MoS_2 on SiO_2/Si was grown by chemical vapor deposition (CVD), while monolayer MoS_2 on Au was prepared by mechanical exfoliation [24,37]. The optical images of MoS_2/SiO_2 and MoS_2/Au are shown in Fig. S1 in the Supplemental Material [36]. The SFG geometry employed in experiment is illustrated in Fig. 1: two laser pulses, both in the same plane normal to the surface, with photon energies of 1.57 and 0.41 eV, were spatially and temporally overlapped at the sample surface and the azimuthal-dependent intensity of the emitted sum frequency pulse was detected. The incident beam energies were chosen such that sum frequency photon energies cover the *A* and *B* exciton energies: we perform final state resonant SFG. The visible beam [0.7 μJ/pulse, full width at half maximum (FWHM): 0.003 eV, 1 kHz] and the infrared beam (0.8 μJ/pulse, FWHM: 0.07 eV, 1 kHz) were both propagated in the *X*-*Z* plane and had incident angles of 64° and 46°, respectively. During the azimuthal-dependent measurements, the beam geometry was fixed while the sample was rotated with respect to the surface normal. The polarization of the three beams was individually set to *p* or *s* to obtain different polarization combinations. To determine the absolute value $\chi^{(2)}$ of MoS_2, *z*-cut alpha quartz was used as our reference sample. All measurements were conducted under ambient conditions at the temperature ≈21.5 °C. Detailed descriptions of the sample preparation, laser system, and optical setup can be found in our previous work [24,37–39] and the Supplemental Material [36].

To better understand the effects of metal substrate on MoS_2, the properties of monolayer MoS_2 on the dielectric substrate, i.e., on SiO_2, were first investigated. Figure 2 shows the integrated SFG intensities measured under the eight different polarization combinations as a function of azimuthal angle. The typical SFG intensities vary with rotation angles as can be seen in Fig. S2 in the Supplemental Material [36]. Virtually all prior work exploring the nonlinear optical response of MoS_2 describes the second harmonic generation using a single incident laser beam and a sixfold symmetric pattern of I_{SHG} with respect to azimuthal angle [32–35]. As shown in Fig. 2, we observed a similar sixfold pattern under all polarization conditions.

As discussed above in the single-beam, I_{SHG} measurement, the polarizations of the two incident interactions cannot be independently adjusted and thus the ability to probe, in the case of both D_{3h} and C_{3v} symmetric systems, four of the eight polarization combination components are lost (see Tables II and I). These additional four observables allow us to gain physical insight beyond that of the SHG measurement. In detail: among all the eight patterns, the SFG intensities show the maximum at the same azimuthal angles (53°, 113°, 173°, 233°, 293°, and 353°) when polarization combinations are *ppp*, *pss*, *ssp*, and *sps* (where the even number of the laser beams are *s*-polarized, group 1), while the corresponding azimuthal angles of the maximum intensities shift by 30° when the polarization combinations are *pps*, *psp*, *spp*, and *sss* (where the odd number of the laser beams are *s*-polarized, group 2). Since our sample was randomly placed on rotation stage, there is always an offset angle (θ_0) between the zigzag direction of MoS_2 and the *p* polarization in the laboratory frame. The detail is mentioned in the global fitting details section in the Supplemental Material [36].

In order to compare the relative magnitudes of SFG intensities under eight polarization combinations, we fitted the measured intensities with the expression in Eq. (6) and used the maximum intensity (I_{max}) of the sixfold petal of the *ppp* polarization to normalize the intensity of the other seven

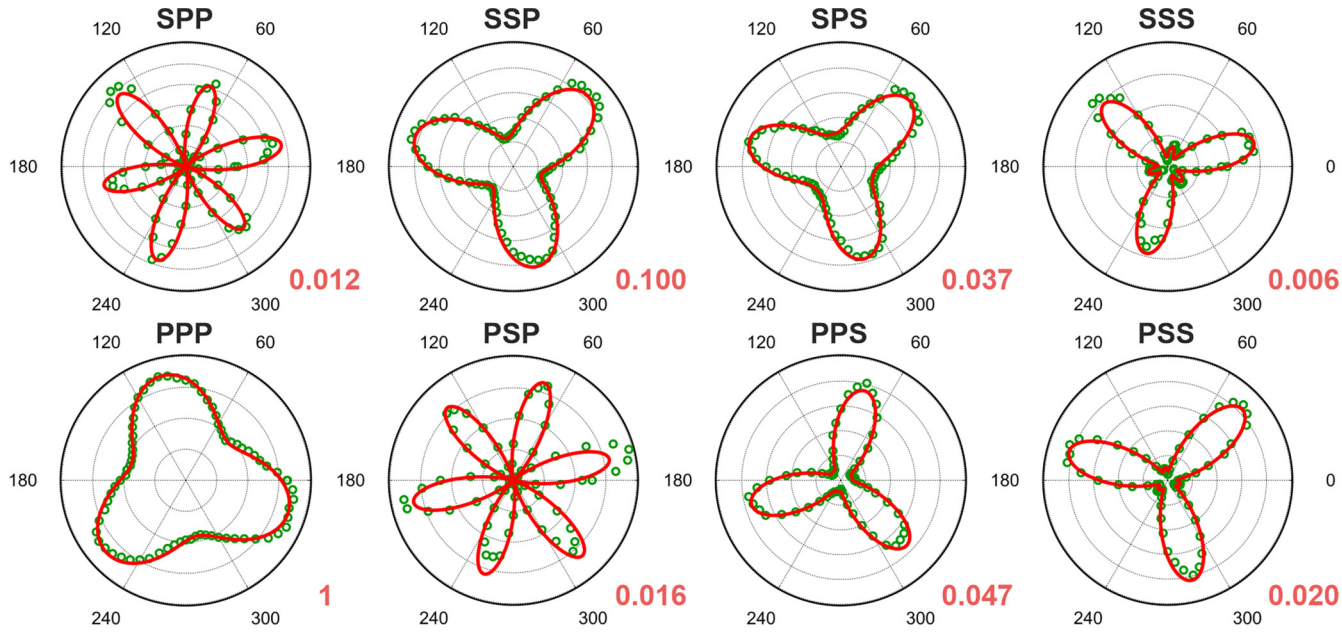

FIG. 3. Azimuthal-dependent SFG intensity of exfoliated monolayer MoS_2 on Au under different polarization combinations. The green circles represent the integrated intensity at specific rotation angles and the red solid lines are the fitting results based on the relative intensity difference analysis. The numbers in the lower right are the relative ratios of the maximum intensity to that of the *ppp* polarization combination.

polarization combinations. For *psp*, *pps*, and *pss* polarizations, the maximum intensity is 1.04, 1.10, and 1.28 times larger than that for *ppp* polarization, respectively, while for *spp*, *ssp*, *sps*, and *sss* polarizations, the ratio of fitting maximum to those of the *ppp* polarization is 0.46, 0.52, 0.55, and 0.58, respectively.

To understand the shift in the azimuthal angle of the maximum intensities between polarization combinations group 1 and group 2 and the polarization-dependent intensities, we calculated the nonzero macroscopic susceptibility tensor under rotation conditions based on a theoretical model including the lattice symmetry of MoS_2, the Euler transformation matrix between molecular and laboratory frames, the linear Fresnel factors and experimental parameters such as the beam incident angles, and interferences due to the film thickness (see the Supplemental Material for details [36]) [40,41]. The results show that the 30° difference in phase between group 1 and group 2 is a straightforward consequence of the inclusion of $\sin(3\theta)$ in some $\chi^{(2)}$ elements and $\cos(3\theta)$ in others (see Table I). The calculation also shows that rationalizing the differences in intensity ratios requires accounting for the Fresnel factors including the interference of the multiply reflected and transmitted SFG beams inside the SiO_2 film between MoS_2 and the Si substrate [42] (the interference process is illustrated in Fig. S3 in the Supplemental Material [36]). As we show in Fig. S4 in the Supplemental Material [36] we simulated the intensity ratios to change as a function of oxide layer thickness: a result that can be quantitatively understood by the description of intraoxide SFG interference. The model predicts that the ratio of *spp* to *ppp* is ≈0.5 when the oxide layer thickness is ≈270 nm, which agrees well with the measured data. A similar thickness-dependent interference effect on Si/SiO_2 substrates was recently reported by Miao [43] *et al.* at different excitation wavelengths in a SHG study.

As shown in Fig. 2, the SFG intensities are well predicted by the global fitting process based on this theoretical model: for given beam angles and polarizations all data can be correctly described by a single $\chi^{(2)}$. The details of this global fitting can be found in the Supplemental Material [36]. These results confirm the inherent symmetry (D_{3h}) of monolayer MoS_2 and the negligible influence on the measured optical response from the dielectric substrate, except for the interference effect. More importantly, our eight independent observations allow determination of the size of the second-order susceptibility in the *A* and *B* exciton frequency region with relatively high precision. Combined with the reference sample, *z*-cut alpha quartz, the only independent nonvanishing element $\chi^{(2)} = \chi^{(2)}_{yyy} = -\chi^{(2)}_{yxx} = -\chi^{(2)}_{xxy} = -\chi^{(2)}_{xyx}$ was found to be $(7.9 \pm 1.6) \times 10^{-20}$ m^2/V (at SFG photon energy of 1.98 eV) for monolayer MoS_2 on SiO_2. This value is comparable to those previously reported for CVD-grown monolayer MoS_2 in a similar energy region [34,44].

With the behavior of monolayer MoS_2 on SiO_2/Si well understood, the properties of MoS_2 on the gold substrate were investigated using the same approach. As shown in Fig. 3, the azimuthal-dependent sum frequency response shows dramatic differences compared to the results on the SiO_2 substrate. While a sixfold symmetric pattern is observed in the *psp* and *spp* polarization combinations for MoS_2 on Au, the remaining six polarization combinations all show a threefold symmetric pattern with detailed features that are polarization dependent. Specifically, the threefold patterns can be categorized into three groups based on shape and *R* ratio ($R = \frac{I_{max}}{I_{min}}$, where I_{min} refers to the minimum intensity): (1) broad petals with a small *R* ratio (*ppp*), (2) medium petals with a moderate *R* ratio (*ssp* and *sps*), and (3) narrow petals with additional small petals in between and a large *R* ratio (*sss*, *pps*, and *pss*). In addition, the absolute size of I_{max} varies significantly between polarization

TABLE III. Results for relative ratios of respective nonzero elements $\chi_i^{(2)}$ probed in laboratory frame to $\chi_{yyy}^{(2)}$ of MoS_2/SiO_2.

Azimuthal-dependent (B)		Azimuthal-independent (A_i)			
Sample	$\chi_{yyy}^{(2)}$	$\chi_{xxz}^{(2)}$ (ssp)	$\chi_{xzx}^{(2)}$ (sps)	$\chi_{zxx}^{(2)}$ (pss)	$\chi_{zzz}^{(2)}$ (ppp)
PVD Au ($C_{\infty v}$)	–	27.55 ± 0.19	3.03 ± 0.02	1.74 ± 0.01	-12.31 ± 0.12
MoS_2/SiO_2 (D_{3h})	1.00	–	–	–	–
MoS_2/Au (C_{3v})	1.82 ± 0.01	9.09 ± 0.03	20.48 ± 0.16	-30.21 ± 0.82	196.09 ± 6.20

combinations: a difference of two orders of magnitude (the maximum in *sss* to that of *ppp* is 0.006).

Because the main distinction between MoS_2/SiO_2 and MoS_2/Au is the substrate it seems reasonable to ask whether the threefold pattern we observe is the nature of an unmodified Au response. We tested this possibility by conducting the same measurements on a PVD gold substrate without MoS_2 under different polarization combinations (Fig. S5 in the Supplemental Material [36]). All observed patterns show an SFG response that is isotropic with respect to changing azimuthal angles for these PVD gold films. We thus conclude that the threefold symmetry of the I_{SFG} response of MoS_2 on Au is not due to the unperturbed optical response of the PVD gold substrate.

To understand the structural implications of the threefold symmetric response, further data analysis is required. There are two possibilities to explain the observed threefold symmetric pattern: the simple coherent superposition of the contributions from the MoS_2 monolayer and the gold substrate or the contributions from a mutually modified system consisting of MoS_2 and Au. The details will be discussed below.

As noted above, for a sample with C_{3v} symmetry along the surface normal the azimuthal dependence of I_{SFG} can be described by Eq. (7): as a coherent superposition of an azimuthal-dependent part ($B\cos 3\theta$ or $B\sin 3\theta$) and azimuthal-independent part (A). Using this functional form and calculating possible responses (Fig. S6 in the Supplemental Material [36]) suggests that the change of symmetric pattern from sixfold to threefold (with respect to azimuthal angle) occurs when A exists and is sufficiently large relative to B. As noted above no azimuthal-independent contribution, i.e., no A, is necessary to describe the optical response of MoS_2 on SiO_2/Si: the measured signal in that system is well described by Eq. (6). As shown in Table I, the existence of an azimuthally independent component of I_{SFG} is not possible for samples belonging to the D_{3h} point group. In what follows we offer a physically motivated argument that placing MoS_2 on Au converts its apparent symmetry from D_{3h} to C_{3v}, describe how, in theory, such a transition would be expected to influence the observables, and assess the relative agreement between the observations and theory.

The D_{3h} point group has one C_3 rotational axis, three C_2 rotational axes, three vertical mirror planes (σ_v), and one horizontal mirror plane (σ_h) perpendicular to the C_3 rotational axis [45]. If the atoms in the top and bottom planes of MoS_2 experience a sufficiently different local environment, the three C_2 rotational axes and σ_h plane will not exist. Removing these point symmetry operators means the system now belongs to C_{3v} or further to the C_3 point group (by also removing the three σ_v planes). Because it involves less structural perturbation, the expected I_{SFG} response of a system with C_{3v} symmetry was examined first. The nonzero macroscopic susceptibility tensor elements of the C_{3v} point group under rotation conditions are shown in Table II. As indicated, it is clear that I_{SFG} measured from a sample with C_{3v} symmetry consists of one independent azimuthal-dependent element ($\chi^{(2)} = \chi_{yyy}^{(2)} = -\chi_{yxx}^{(2)} = -\chi_{xxy}^{(2)} = -\chi_{xyx}^{(2)}$) and four azimuthal-independent elements ($\chi_{xxz}^{(2)}$, $\chi_{xzx}^{(2)}$, $\chi_{zxx}^{(2)}$, and $\chi_{zzz}^{(2)}$) [46]. The simulated patterns under different polarization combinations are shown in Fig. S7 in the Supplemental Material [36]. As we showed there, this analysis clearly rationalizes the observed trends in the data with the exception of the azimuthal pattern observed under the *pps* and *sss* polarization combinations. Here theoretical considerations predict a sixfold symmetry instead of the observed threefold. As we showed in the Supplemental Material [36], this change can be rationalized by a small polarization impurity in the broadband infrared beam created by the half waveplate and with heightened influence due to the large effective second-order susceptibility components probed by the p-polarized infrared. See the Supplemental Material [36] for a quantitative estimate of the contribution of the polarization impurity to our measured signal and a general discussion of the role of the relative size of the susceptibility components in making this effect apparent.

While it thus appears our results can be understood as a result of a sample system with C_{3v} symmetry, it is worth noting (as mentioned above) that the symmetry allowed components of the susceptibility of materials in the C_{3v} point group are exactly the same as those that have a combination of D_{3h} and $C_{\infty v}$ (see Table SI in the Supplemental Material [36]). In order to distinguish the two scenarios we first extracted the relative ratios of respective nonzero $\chi_i^{(2)}$ probed in the laboratory frame for a gold substrate and MoS_2/Au with respect to the $\chi_{yyy}^{(2)}$ of MoS_2 on SiO_2. As noted in detail in Table SII in the Supplemental Material [36], this comparison requires quantitatively accounting for the Fresnel coefficients for both azimuthal-dependent and -independent $\chi^{(2)}$ terms and their dramatic change with polarization. The results of this analysis are shown in Table III. For the gold substrate ($C_{\infty v}$) and hexagonal MoS_2 response (D_{3h}) the signal consists of four out-of-plane azimuthal-independent elements ($\chi_{xxz}^{(2)}$, $\chi_{xzx}^{(2)}$, $\chi_{zxx}^{(2)}$, and $\chi_{zzz}^{(2)}$), measured on the PVD gold substrate without MoS_2, and one in-plane azimuthal-dependent element ($\chi_{yyy}^{(2)} = -\chi_{yxx}^{(2)} = -\chi_{xxy}^{(2)} = -\chi_{xyx}^{(2)}$), measured in the MoS_2 on SiO_2/Si system. While all five components are present in the MoS_2 on Au sample, it is clear that the relative sizes of the components differ significantly in the two scenarios. For example, the size of the azimuthal-independent element $\chi_{xxz}^{(2)}$ for PVD Au is three times larger than that for MoS_2/Au. We thus conclude that the results shown in Table III are inconsistent

with a scenario in which our optical response is the coherent sum of pure Au and, relatively unperturbed, MoS_2; we rather observe a gold-modified MoS_2 system.

As for the MoS_2 on SiO_2/Si system we also extracted the quantitative value of $\chi^{(2)}_{yyy}$ for MoS_2/Au and found it to be $(1.4 \pm 0.3) \times 10^{-19}$ m^2/V (at SFG photon energy of 1.98 eV) or $\approx 2\times$ that of MoS_2 on SiO_2/Si. The enhancement can result from the modification by the gold substrate or the higher quality of exfoliated monolayer MoS_2 than the CVD-grown one [34]. Regardless of the physical origin of this effect, it seems clear that the quantitative description of the $\chi^{(2)}$ of monolayer MoS_2 is a prerequisite in the realization of 2D devices by knowing their azimuthal-dependent optical response.

The fact that the symmetry of the optical response of MoS_2 changes from point group D_{3h} to C_{3v} after it is placed on the gold surface suggests a strong interaction between MoS_2 and gold. That the MoS_2/Au interaction is stronger than the interlayer van der Waals forces within the bulk MoS_2 is often suggested to explain the relative ease with which monolayer MoS_2 can be exfoliated onto gold [24,47]. From a microscopic perspective, we imagine two possible strong interactions that may contribute to the evolution of symmetry of monolayer MoS_2: (1) the formation of Au-S covalent bonds at the interface leads to changes in the crystalline structure, i.e., Mo-S bond distances of monolayer MoS_2 or(/and) (2) charge transfer from the gold substrate results in the changes in the electronic structure of monolayer MoS_2. Recently, several DFT studies have shown, consistent with experiment, that the average distance between the S atoms in the bottom layer and Au atoms in the top layer is larger than the typical value of the Au-S covalent bond [47–49]. These results suggest that the interaction between MoS_2 and Au is somewhat less strong than Au-S covalent bonding and similar to the recently reported noncovalent interaction, which resembles covalent quasibonding [50]. While Au-S covalent bonds can exist between MoS_2 and a gold substrate, they generally appear to be mediated by Au defects [47,49]. While the interaction strength between a pristine Au surface and MoS_2 monolayer is less strong than expected from covalent bonding, several theoretical [49,51,52] and experimental studies [48,53] have confirmed the existence of charge transfer from the Au substrate to MoS_2 and that the charge redistribution modulates the electronic structure of MoS_2 while causing limited lattice distortion.

Here we can directly exclude the structural changes by measuring the azimuthal response at different SFG (SHG) photon energies. As shown in Fig. 4, compared with the threefold symmetry for *ssp* polarization combination already shown in Fig. 3, a sixfold symmetric pattern was observed for MoS_2/Au at SFG (SHG) photon energy of 3.12 eV, confirming that the symmetry of the optical response of MoS_2 changes from D_{3h} to C_{3v} point group after it is placed on the gold surface because of a mode-specific (depending on exciton resonance) electronic effect.

Recent results [53] also indicate that the charge transfer from a metal substrate and lattice strain could induce a phase transition of monolayer TMDC from semiconductor to metal, e.g., from the 2H phase of MoS_2 to the 1T phase. Since the 1T monolayer MoS_2 belongs to a centrosymmetric point group, it is not expected to show an SFG response by the symmetry selection rules of the process. Our SFG results thus directly confirm that monolayer MoS_2 on a gold substrate in the air does not undergo this phase change. The ability to characterize the symmetry of the I_{SFG} optical response and relate it to the TMDC phase is a noninvasive means of structural characterization only offered by this, or analogous, nonlinear optical approaches.

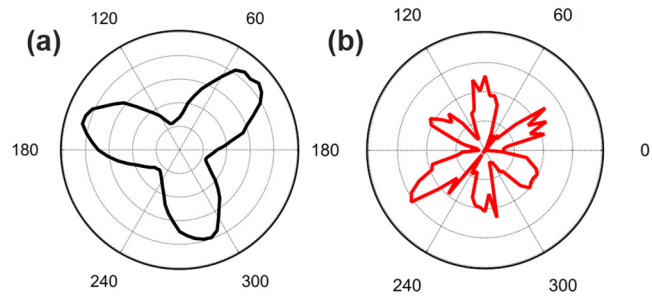

FIG. 4. Azimuthal-dependent SFG (SHG) intensity of exfoliated monolayer MoS_2 on Au at SFG (SHG) photon energies of (a) 1.98 eV and (b) 3.12 eV under the *ssp* polarization combination.

IV. CONCLUSION

Completely different symmetries of the optical response of MoS_2 were observed on Au compared to the always reported sixfold symmetry on a dielectric substrate, suggesting a strong interaction between the metal substrate and MoS_2. The absolute values of azimuthal-dependent $\chi^{(2)}$ of monolayer MoS_2 on SiO_2 and Au were extracted in the *A* and *B* exciton regions and have the size of $(7.9 \pm 1.6) \times 10^{-20}$ and $(1.4 \pm 0.3) \times 10^{-19}$ m^2/V, respectively. These values are comparable to those previously reported for CVD-grown monolayer MoS_2 and exfoliated monolayer MoS_2 and can be used as an important reference for the design of 2D optoelectronic devices. The apparent symmetry change when monolayer MoS_2 is placed on a gold substrate compared to a SiO_2 substrate has been well understood as a mode-specific electronic effect rather than a geometric structural change. Our study provides a deeper understanding of the strong interaction between monolayer TMDCs and metal substrates and the significant modulation of the NLO response by a metal, which offers the possibility of fabricating high-performance devices by combining the azimuthal-dependent optical responses and substrate modification.

ACKNOWLEDGMENTS

This work was funded by the Deutsche Forschungsgemeinschaft (DFG, German Research Foundation) through Projects A06, B02, and C05 of the Collaborative Research Center SFB 1242 "Non-Equilibrium Dynamics of Condensed Matter in the Time Domain" (Project No. 278162697), through Germany's Excellence Strategy (EXC 2033 - 390677874 - RESOLV) and through SCHL 384/20-1 (Project No. 406129719). Additional support was provided by the European Research Council, i.e., ERC-CoG-2017 SOLWET (Project No. 772286) to R.K.C.

[1] Q. H. Wang, K. Kalantar-Zadeh, A. Kis, J. N. Coleman, and M. S. Strano, Nat. Nanotechnol. **7**, 699 (2012).

[2] Z. Yin, H. Li, H. Li, L. Jiang, Y. Shi, Y. Sun, G. Lu, Q. Zhang, X. Chen, and H. Zhang, ACS Nano **6**, 74 (2012).

[3] K. Ullah, Y. Meng, Y. Shi, and F. Wang, Adv. Opt. Mater. **10**, 2101860 (2022).

[4] A. R. Khan, L. Zhang, K. Ishfaq, A. Ikram, T. Yildrim, B. Liu, S. Rahman, and Y. Lu, Adv. Funct. Mater. **32**, 2105259 (2022).

[5] X. Zou and Y. Zhang, Chem. Soc. Rev. **44**, 5148 (2015).

[6] A. Ali, F. A. Mangrio, X. Chen, Y. Dai, K. Chen, X. Xu, R. Xia, and L. Zhu, Nanoscale **11**, 7813 (2019).

[7] T. Goswami, R. Rani, K. S. Hazra, and H. N. Ghosh, J. Phys. Chem. Lett. **10**, 3057 (2019).

[8] C. Xu, H. W. Yong, J. He, R. Long, A. R. Cadore, I. Paradisanos, A. K. Ott, G. Soavi, S. Tongay, G. Cerullo, A. C. Ferrari, O. V. Prezhdo, and Z.-H. Loh, ACS Nano **15**, 819 (2021).

[9] R. Kappera, D. Voiry, S. E. Yalcin, B. Branch, G. Gupta, A. D. Mohite, and M. Chhowalla, Nat. Mater. **13**, 1128 (2014).

[10] S. McDonnell, R. Addou, C. Buie, R. M. Wallace, and C. L. Hinkle, ACS Nano **8**, 2880 (2014).

[11] A. Allain, J. Kang, K. Banerjee, and A. Kis, Nat. Mater. **14**, 1195 (2015).

[12] N. Krane, C. Lotze, J. M. Läger, G. Reecht, and K. J. Franke, Nano Lett. **16**, 5163 (2016).

[13] M. Drüppel, T. Deilmann, P. Krüger, and M. Rohlfing, Nat. Commun. **8**, 2117 (2017).

[14] I. Popov, G. Seifert, and D. Tomanek, Phys. Rev. Lett. **108**, 156802 (2012).

[15] J. Kang, W. Liu, D. Sarkar, D. Jena, and K. Banerjee, Phys. Rev. X **4**, 031005 (2014).

[16] Y. Wang, J. C. Kim, R. J. Wu, J. Martinez, X. Song, J. Yang, F. Zhao, A. Mkhoyan, H. Y. Jeong, and M. Chhowalla, Nature (London) **568**, 70 (2019).

[17] A. Grillo, A. Di Bartolomeo, F. Urban, M. Passacantando, J. M. Caridad, J. Sun, and L. Camilli, ACS Appl. Mater. Interfaces **12**, 12998 (2020).

[18] Y. Yu, Z. Ji, S. Zu, B. Du, Y. Kang, Z. Li, Z. Zhou, K. Shi, and Z. Fang, Adv. Funct. Mater. **26**, 6394 (2016).

[19] K. Wang, J. Wang, J. Fan, M. Lotya, A. O'Neill, D. Fox, Y. Feng, X. Zhang, B. Jiang, Q. Zhao, H. Zhang, J. N. Coleman, L. Zhang, and W. J. Blau, ACS Nano **7**, 9260 (2013).

[20] K. F. Mak, C. Lee, J. Hone, J. Shan, and T. F. Heinz, Phys. Rev. Lett. **105**, 136805 (2010).

[21] A. Splendiani, L. Sun, Y. Zhang, T. Li, J. Kim, C.-Y. Chim, G. Galli, and F. Wang, Nano Lett. **10**, 1271 (2010).

[22] N. Scheuschner, O. Ochedowski, A.-M. Kaulitz, R. Gillen, M. Schleberger, and J. Maultzsch, Phys. Rev. B **89**, 125406 (2014).

[23] U. Bhanu, M. R. Islam, L. Tetard, and S. I. Khondaker, Sci. Rep. **4**, 5575 (2015).

[24] E. Pollmann, S. Sleziona, T. Foller, U. Hagemann, C. Gorynski, O. Petri, L. Madauß, L. Breuer, and M. Schleberger, ACS Omega **6**, 15929 (2021).

[25] Z. Li, Y. Xiao, Y. Gong, Z. Wang, Y. Kang, S. Zu, P. M. Ajayan, P. Nordlander, and Z. Fang, ACS Nano **9**, 10158 (2015).

[26] G. Yi Jia, Q. Zhang, Z. Xian Huang, S. Bin Huang, and J. Xu, Phys. Chem. Chem. Phys. **19**, 27259 (2017).

[27] Y. Li, Y. Rao, K. F. Mak, Y. You, S. Wang, C. R. Dean, and T. F. Heinz, Nano Lett. **13**, 3329 (2013).

[28] A. Autere, H. Jussila, Y. Dai, Y. Wang, H. Lipsanen, and Z. Sun, Adv. Mater. **30**, 1705963 (2018).

[29] Y. Zhang, D. Huang, Y. Shan, T. Jiang, Z. Zhang, K. Liu, L. Shi, J. Cheng, J. E. Sipe, W.-T. Liu, and S. Wu, Phys. Rev. Lett. **122**, 047401 (2019).

[30] K.-Q. Lin, S. Bange, and J. M. Lupton, Nat. Phys. **15**, 242 (2019).

[31] A. Strasser, H. Wang, and X. Qian, Nano Lett. **22**, 4145 (2022).

[32] N. Kumar, S. Najmaei, Q. Cui, F. Ceballos, P. M. Ajayan, J. Lou, and H. Zhao, Phys. Rev. B **87**, 161403(R) (2013).

[33] L. M. Malard, T. V. Alencar, A. P. M. Barboza, K. F. Mak, and A. M. de Paula, Phys. Rev. B **87**, 201401(R) (2013).

[34] D. J. Clark, V. Senthilkumar, C. T. Le, D. L. Weerawarne, B. Shim, J. I. Jang, J. H. Shim, J. Cho, Y. Sim, M.-J. Seong, S. H. Rhim, A. J. Freeman, K.-H. Chung, and Y. S. Kim, Phys. Rev. B **90**, 121409(R) (2014).

[35] L. Mennel, M. M. Furchi, S. Wachter, M. Paur, D. K. Polyushkin, and T. Mueller, Nat. Commun. **9**, 516 (2018).

[36] See Supplemental Material at http://link.aps.org/supplemental/10.1103/PhysRevB.107.155433 for details about coordinate transformation,global fitting,impurity discussion,simulation of symmetric patterns, and the values of Fresnel factors.

[37] E. Pollmann, L. Madauß, S. Schumacher, U. Kumar, F. Heuvel, C. vom Ende, S. Yilmaz, S. Güngörmüs, and M. Schleberger, Nanotechnology **31**, 505604 (2020).

[38] Y. Tong, F. Lapointe, M. Thämer, M. Wolf, and R. K. Campen, Angew. Chem., Int. Ed. **56**, 4211 (2017).

[39] Y. Tong, I. Y. Zhang, and R. K. Campen, Nat. Commun. **9**, 1313 (2018).

[40] A. G. Lambert, Ph.D. thesis, University of Cambridge, 2001.

[41] X.-H. Hu, F. Wei, H. Wang, and H.-F. Wang, J. Phys. Chem. C **123**, 15071 (2019).

[42] Y. Tong, Y. Zhao, N. Li, M. Osawa, P. B. Davies, and S. Ye, J. Chem. Phys. **133**, 034704 (2010).

[43] X. Miao, N. Xuan, Q. Liu, W. Wu, H. Liu, Z. Sun, and M. Ji, ACS Appl. Mater. Interfaces **9**, 34448 (2017).

[44] C. T. Le, D. J. Clark, F. Ullah, V. Senthilkumar, J. I. Jang, Y. Sim, M.-J. Seong, K.-H. Chung, H. Park, and Y. S. Kim, Ann. Phys. (Leipzig) **528**, 551 (2016).

[45] N. Colthup, *Introduction to Infrared and Raman Spectroscopy* (Elsevier, Amsterdam, 2012).

[46] R. W. Boyd, *Nonlinear Optics* (Academic Press, New York, 2020).

[47] M. Velický, G. E. Donnelly, W. R. Hendren, S. McFarland, D. Scullion, W. J. I. DeBenedetti, G. C. Correa, Y. Han, A. J. Wain, M. A. Hines, D. A. Muller, K. S. Novoselov, H. D. Abruña, R. M. Bowman, E. J. G. Santos, and F. Huang, ACS Nano **12**, 10463 (2018).

[48] F. Tumino, C. S. Casari, A. Li Bassi, and S. Tosoni, J. Phys. Chem. C **124**, 12424 (2020).

[49] S. Sarkar and P. Kratzer, J. Phys. Chem. C **125**, 26645 (2021).

[50] Y. Huang, Y.-H. Pan, R. Yang, L.-H. Bao, L. Meng, H.-L. Luo, Y.-Q. Cai, G.-D. Liu, W.-J. Zhao, Z. Zhou, L.-M. Wu, Z.-L. Zhu, M. Huang, L.-W. Liu, L. Liu, P. Cheng, K.-H. Wu, S.-B. Tian, C.-Z. Gu, Y.-G. Shi, Y.-F. Guo, Z. G. Cheng, J.-P. Hu, L. Zhao, G.-H. Yang, E. Sutter, P. Sutter, Y.-L. Wang,

W. Ji, X.-J. Zhou, and H.-J. Gao, Nat. Commun. **11**, 2453 (2020).

[51] H. Zhong, R. Quhe, Y. Wang, Z. Ni, M. Ye, Z. Song, Y. Pan, J. Yang, L. Yang, M. Lei, J. Shi, and J. Lu, Sci. Rep. **6**, 21786 (2016).

[52] B. Ouyang, S. Xiong, and Y. Jing, npj 2D Mater. Appl. **2**, 13 (2018).

[53] F. Wu, Z. Liu, N. Hawthorne, M. Chandross, Q. Moore, N. Argibay, J. F. Curry, and J. D. Batteas, ACS Nano **14**, 16939 (2020).